Bulletin of the Seismological Society of America, Vol. 85, No. 4, pp. 1003–1020, August 1995

A Complex Double-Couple Source Mechanism for the M_S 7.2 1929 Grand Banks Earthquake

by Allison L. Bent

Abstract The M_S 7.2 Grand Banks earthquake of 1929 was one of the largest and the most fatal earthquakes to have occurred in Canada, with most of the death and destruction having been caused by a tsunami and submarine landslide associated with the earthquake. It has been suggested (Hasegawa and Kanamori, 1987) that a single-force (landslide) mechanism was more consistent with the data than was a double-couple source and that therefore the event was not an earthquake. However, that particular study considered only four double-couple solutions and left many unanswered questions, in particular with respect to the source time function and sediment volume involved. Here, a larger number of seismograms are used to examine the full range of double-couple solutions to determine more definitively the nature of the event. Waveform modeling using both forward and inverse methods indicates that this event was an earthquake, with a complex source mechanism. The first and largest subevent was a strike-slip double-couple event occurring on a northwest-striking plane. Two later subevents were probably strike-slip double couples on northeast-striking planes, but other mechanisms cannot be completely ruled out. The first subevent has a well-constrained focal depth of 20 $\pm$ 2 km. The second and third subevents also appear to have occurred at 20 km, but are constrained only to within ± 5 km. These depths provide further evidence that the event was not a landslide. The sum of the subevent moments corresponds to an M_W of 7.2 $\pm$ 0.3, which is in close agreement with the M_W of 7.1 $\pm$ 0.1 obtained by the CMT method using long-period data. These M_W's are also consistent with the M_S of 7.2 (± 0.3) and m_B of 7.1 (± 0.2) calculated directly from the seismograms. Modeling of the seafloor displacement for this mechanism indicates that the tsunami was generated by the landslide and not directly by the earthquake.

Introduction

The M_S 7.2 Grand Banks earthquake of 18 November 1929 (Fig. 1), which occurred off the coast of eastern Canada in the Laurentian Channel near the top of the continental slope, was the largest instrumentally recorded earthquake to have occurred in southeastern Canada and was responsible for 27 of the 28 known earthquake-related deaths in Canada. It was unusual for this part of the world in that it was associated with a tsunami and large-scale submarine slumping. The slumping extended as much as 250 km from the epicenter and consisted of the movement of roughly 10^{11} m^3 of sediment down the continental slope (Piper and Aksu, 1987). The shaking was widely felt in Nova Scotia, Newfoundland, and the northeastern United States. Most of the property damage and all of the fatalities, mostly in southern Newfoundland, were caused by the tsunami (Doxsee, 1948), and numerous breaks to trans-Atlantic telephone cables were attributed to the submarine slump and resulting turbidity current.

Until the 1980s it was assumed that the submarine slump was triggered by the earthquake. Gussow (1982) suggested, however, that the slump may have been the triggering mechanism, and more recently, Hasegawa and Kanamori (1987) concluded that the seismograms were more compatible with a single-force mechanism than with a double-couple mechanism, implying that the seismic signal was generated by the slump and not by an earthquake (although they could not rule out a slump triggered by a smaller earthquake). However, their study left many unresolved questions, several of which have been raised previously, in particular by Adams and Basham (1989). These questions are briefly summarized below.

First, although the single-force mechanism provided a better fit to the data than the double-couple solutions tested, only four double-couple mechanisms were considered, thus raising the possibility that there could be an untested double-couple solution consistent with the observations. Also, al-

though surface-wave spectra at two stations (at nearly the same azimuth and distance from the epicenter) were examined, the landslide interpretation was based very heavily on first-motion (*P* and *S*) data from only a portion of the available seismograms. In addition, the resulting mechanism was not tested for its fit to the overall waveforms.

Second, the volume of sediment required to produce the force determined by Hasegawa and Kanamori (1987) (5.5×10^{11} m^3) is five to 10 times the volume of the slump computed from *in situ* measurements (Piper and Aksu, 1987). Hasegawa and Kanamori (1987), although aware of these measurements, argued, not without some validity, that this is a difficult parameter to measure precisely. However, recent studies of the seafloor bottom and analyses of the sediment material (Piper and Aksu, 1987; Piper *et al.*, 1988) have suggested that only some (5 to 10%) of the material deposited after the 1929 event came from slumping of the continental slope, and that much of the sediment originated from the fan valleys at the base of the continental slope, and consisted of material that was probably liquefied during the shaking and then transported. Furthermore, Hughes Clarke (1990) has found evidence that the sediment from the fan valleys was deposited after the deposition of the sediment slumped from the continental slope, although he could not determine a precise time scale—only that it was from a few minutes to several hours later. These studies all suggest that the volume of sediment slumped was too small by a factor of perhaps 100 or more to have produced the observed ground vibrations attributed to the 1929 earthquake.

Third, the seismograms contain considerable high-frequency energy. A large volume of sediment is unlikely to be able to slump quickly enough to produce these high-frequency signals. In a related objection to the landslide mechanism, there was no significant difference between m_B calculated at intermediate periods and M_S and M_W calculated at long periods, which implies that the event was not enriched in long-period energy, which would have been expected if the slump had made a significant contribution to the recorded waveforms (unless it truly was instantaneous). In addition, an epicenter was computed for the event, suggesting it was a sudden high-energy event rather than a slowly propagating slump, whereas Piper *et al.* (1985) found that the origin of the slump could not be attributed to a point source but was spread over a 50-km radius in the region of the 1929 epicenter.

Of course, although the above arguments favor a double-couple source, none of them prove that the event was not a landslide. However, they do suggest that a more detailed source study using all of the available data is war-

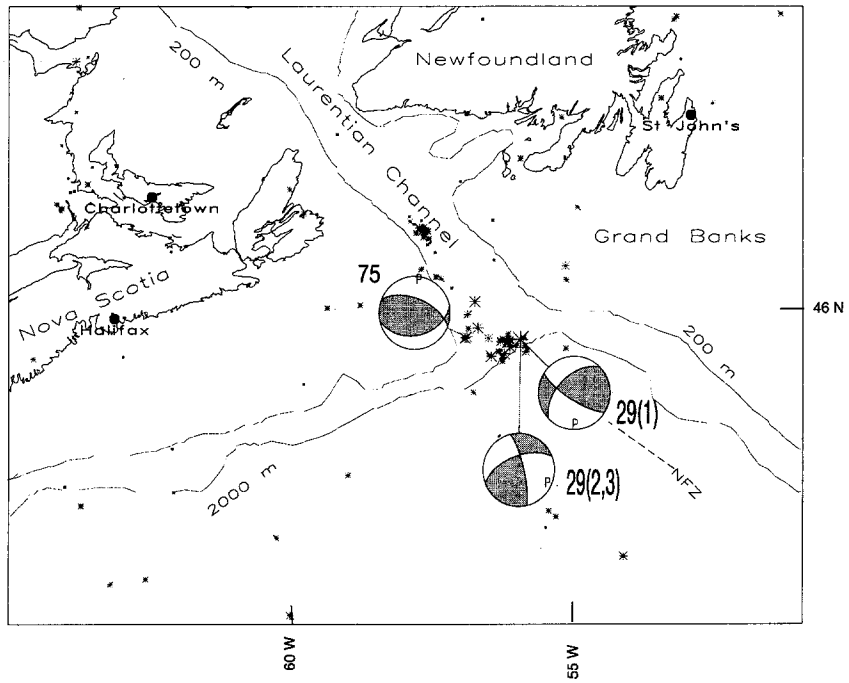

Figure 1. Seismicity in the region of the 1929 Grand Banks earthquake. All located earthquakes from the Geological Survey of Canada earthquake data base of magnitude 2.0 or greater between 1900 and 1993 are shown, with the symbol size scaled to magnitude. For the smallest and oldest earthquakes, the number of recorded earthquakes is probably less than the number of earthquakes that actually occurred. 29(1) refers to the first subevent of the 1929 earthquake; 29(2,3) refers to the second and third subevents; 75 refers to the 1975 Laurentian Channel earthquake (Hasegawa and Herrmann, 1989). NFZ is the Newfoundland Fracture Zone. For reference, the 200 and 2000 m bathymetry contours are shown.

ranted and might provide more convincing evidence for selecting one source type over the other.

The primary goals of this study are 2-fold: to use waveform modeling to explore a wider range of potential double-couple solutions to resolve more definitively whether the slumping was triggered by the earthquake or whether, in effect, the slumping was the "earthquake," and then to provide a well-constrained set of source parameters for the preferred mechanism. The resolution of these questions will have implications for the seismic hazard assessment and recurrence interval estimates in this region as the return period for large-scale slumping, which requires large sediment accumulations, could be longer than that for a tectonic earthquake. Improved seismic hazard evaluations are desirable not only for onshore regions within the potential felt area of future events, but also for offshore hydrocarbon exploration facilities. In addition, understanding the tsunami potential is important for the coastal regions of Nova Scotia and Newfoundland.

Regional Seismicity and Seismotectonics

The regional seismotectonics in the area of the 1929 epicenter are not well understood. The two main features are the Laurentian Channel and the continental margin. There are two schools of thought concerning the origin and nature of the Laurentian Channel. Kumarepeli and Saull (1966) and Kumarepeli (1970) have argued that the Laurentian Channel has a tectonic origin and was at one time part of a rift system subparallel to the St. Lawrence Valley, and Drake and Woodward (1963) and Kumarepeli (1970) have used the offset between the Appalachians in New Brunswick and Newfoundland to suggest that there has been active faulting along the Laurentian Channel. In addition, Fletcher *et al.* (1978) have noted that a westward extension of the Newfoundland Fracture Zone would extend through the 1929 epicenter and run more or less parallel to the Laurentian Channel. Williams *et al.* (1972), however, on the basis of geomorphology and seismic reflection studies, have suggested that the Laurentian Channel is an erosional feature, in part related to glacial erosion. The latter is also the interpretation preferred by King and MacLean (1970) and Piper *et al.* (1988).

The tectonics of the continental margin are somewhat better understood, and suggest a complex history. Keen and Haworth (1984a, b) conclude that the continental margin off Nova Scotia was formed by rifting, while the margin off southern Newfoundland, at roughly right angles to the Nova Scotia margin, was transform-fault generated.

Although the overall level of seismic activity in the Laurentian Channel is not particularly high, it is the most active offshore region of southeastern Canada (Fig. 1). The trend of the seismicity in this region parallels the Laurentian Channel but occurs very close to the edge of the continental margin, and it is not clear which (if either) feature is the controlling factor. Excluding the 1929 aftershocks, there are four known earthquakes of magnitude 5.0 or greater in this region (Adams, 1986). Three of them occurred prior to the installation of the WWSSN network and modernization of the Canadian network in the 1960s and therefore were not well recorded or studied. Hasegawa and Herrmann (1989) determined that the 1975 (M 5.2) earthquake was a deep (30 km) subcrustal, predominantly thrust event on a roughly east–west-striking plane.

Data Set

Shortly after the 1929 earthquake, a collection of seismograms from more than 30 seismograph stations was assembled in Ottawa. The data set has recently been augmented by additional records from the former Soviet Union, the western United States, and Sweden and now contains records from 46 stations (summarized in the Appendix, and shown in Fig. 2). Although there is at least one record from every quadrant, the azimuthal coverage and data quality are not uniform. In most cases, the instrument constants were provided by the seismograph station operators at the time they sent the seismograms, and these values probably represent the best estimates of the instrument responses at the time of the earthquake. For those stations that did not send the instrument constants, they were obtained from a number of secondary sources including station bulletins, Charlier and Van Gils (1953), Ebel *et al.* (1986), Street and Turcotte (1977), Wilson (1940), and Wood (1921). The instrument parameters are summarized in the Appendix. A more detailed description of the data set may be found in Bent (1994).

As seen in the Appendix, in some cases the instrument constants for the north and east components at the same station were significantly different. When this occurred and a modeling technique required the seismograms to be rotated, the instrument response was deconvolved from one component and the resulting record was convolved with the instrument response of the other component—usually the longer period instrument. After the instruments were equalized, the horizontal components were rotated. If a technique did not require rotation, the original instrument responses were retained.

The polarities of many of the instruments are difficult to determine with a high degree of certainty. If the polarity was written on the original record it is assumed to be correct unless there are strong reasons to believe otherwise. Hasegawa and Kanamori (1987) made some polarity assumptions for a number of instruments. Their polarity assumptions are assumed to be correct but, in case of conflict, will be abandoned more readily than first motions at stations with marked polarities. Polarities are considered more reliable at azimuths where the data points are both redundant and consistent (for example, Europe). In the source modeling, polarities are taken into consideration but a higher weight is given to a good overall waveform fit than to a first-motion polarity only. This weighting is used in the sense that a synthetic seismogram that is a perfect mirror image of the data

is considered more acceptable than one that fits the assumed first motion, but not the rest of the seismogram. Similarly, a mirror image is preferable to a solution that fits most of the seismogram but not the first motion. It is usually possible from the first motions to determine whether the polarities of the horizontal components at any station are consistent with each other even if they cannot be determined in an absolute sense, so the rotations of the mutually consistent horizontal components should not be adversely affected by any incorrect assumptions about the instrument polarities. In the end, it did not appear that any of the polarity assumptions were incorrect, with the possible exception of MEL, which was not used to determine the solution.

Modeling Techniques

The body waves (both *P* and *S*) were analyzed using a forward modeling technique based on ray summation in the time domain discussed in detail by Langston and Helmberger (1975). Using this method, the observed seismograms (waveform and amplitude) are compared to synthetic seismograms computed for a specific set of source parameters, which are adjusted until a good fit is obtained. A point source is assumed, but source complexity can be simulated by adding together two or more point sources, each with a trapezoidal source time function. For *P* waves the vertical component was modeled when available. Otherwise the radial component was modeled. If only one horizontal component was available, the *P* waveform was modeled but the amplitude was not used in the moment calculations. For *S* waves, the horizontal components were modeled. Where only one component was available, the record was not modeled unless the station was naturally rotated. Records from stations at upper-mantle triplication distances were used only if required for azimuthal coverage because they are more sensitive to the choice of velocity structure than teleseismic waves are. A number of attenuation values were tested. Overall, it was found that a Futterman (1962) operator, t^*, of 1 sec was the most appropriate for both *P* and *S* waves. Although t^* for *S* waves is typically in the 3- to 4-sec range, a value of 1 sec is required for the *P* and *S* waves to be modeled using the same source time function, and is in the range employed in source studies of other eastern North American earthquakes [for example, Ebel *et al.* (1986); Bent (1992)].

A velocity structure appropriate for the Laurentian Channel area was used in the forward modeling. The epicenter occurred in a geologically complex region, which has been approximated here by two flat layered models: one for stations east of the epicenter and another for stations to the west. Two models were used because the epicenter occurred near the edge of the continental slope where the structure is rapidly changing. For stations to the west the model of Reid (1987) based on a refraction survey of the Laurentian Channel was used (Table 1). The velocity model for eastern azimuths (Table 1) is a hybrid of this model and "Line E" from Keen and Hyndman (1979). Both models have the same number and type of layers. The major differences are that the water depth is greater and the Moho is shallower for the eastern model. The ray set modeled included multiple reflections in the water and sediment layers.

The method described above assumes a double-couple

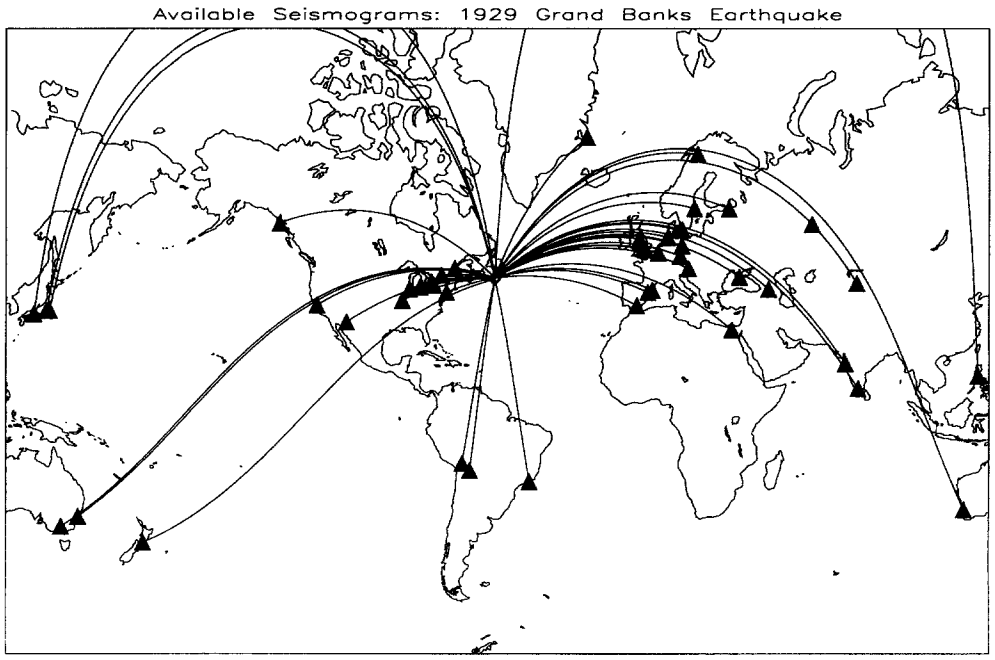

Figure 2. Map showing the seismograph station distribution and great circle paths for the 1929 Grand Banks earthquake. The stations are summarized in the Appendix.

source. To test possible single-force mechanisms, the body waves were modeled in the time domain by replacing the double-couple source term with the single-force source described by Kanamori *et al.* (1984). Otherwise, the parameters are as described above.

The data were also analyzed using the centroid moment tensor (CMT) method described by Dziewonski *et al.* (1981) and Dziewonski and Woodhouse (1983). This method based on the summation of the Earth's normal modes is used to obtain the focal mechanism as well as the source centroid. Unlike the forward modeling technique discussed above, the CMT method does not assume a double-couple source. The long-period body waves were analyzed at two period ranges—greater than 32 sec and greater than 45 sec. Despite the magnitude of the earthquake, long-period mantle waves could not be used in the inversion because the fall-off of the instrument gains with period were such that very little energy was recorded in the 135-sec period range normally used in the inversion. The mantle model of Dziewonski and Woodward (1992), which corrects for long-period lateral variations in velocity, was used in the inversion.

The surface waves were analyzed using the spectral amplitude inversion technique of Herrmann (1979). As for the *S* waves, single-component stations were not used unless they were naturally rotated. Emphasis was placed on the 20- to 40-sec period range. At shorter periods, structural heterogeneities and possible source complexities render the results unreliable, and at longer periods the instrument magnifications were too low to be useful (except at a few high-gain long-period stations where the surface waves were off-scale). Globally averaged attenuation (Tsai and Aki, 1970) and velocity (Dziewonski and Anderson, 1981) models were used because the surface waves generally had mixed continental and oceanic paths. Additionally, the Love- to Rayleigh-wave amplitude ratios were compared to the expected ratios for the various sources proposed for this earthquake.

Source Parameters

First Motions

A first-motion focal mechanism was determined (strike 123°, dip 70°, rake 148°) and used as a starting solution for modeling the waveforms. Because of the difficulties in absolutely determining polarities as discussed earlier, this solution is used only as a starting point. In case of conflict, any solution that provides a good fit to both the body and surface waves, but results in some first-motion inconsistencies, is considered more acceptable than one that fits the assumed first motions but not the waveforms. The first motions listed by Hasegawa and Kanamori (1987) at 14 stations were supplemented by nine additional stations, and were then inverted for the focal mechanism. The first motions are summarized in Table 3. Because the 1975 Laurentian Channel earthquake, which occurred near the 1929 epicenter, occurred at a depth of 30 km (Hasegawa and Herrmann, 1989) the inversion was performed with take-off angles appropriate to both crustal and mantle sources. The results were not strongly depth dependent, and a crustal source mechanism is shown in Figure 3.

The first motions (both *P* and *S* were used) suggest a predominantly strike-slip mechanism with a small thrust component with slip on a plane striking either southeast or southwest. All the European stations appear to be compressional for *P*. Because there are a large number of European stations, it is assumed that Europe is in a compressional quadrant. Eastern and western North American stations appear to be compressional while the two north-central North American stations (AAM, CHI) appear dilatational. There is some redundancy here but not to as great an extent as in

Table 1
Velocity Model

α (km/sec)	β (km/sec)	ρ (g/cm^3)	Thickness (km) (West)	Thickness (km) (East)
1.5	0.0	1.0	2.0	4.0
3.0	1.65	2.25	4.0	3.0
4.25	2.4	2.4	4.0	1.0
5.0	2.89	2.6	5.0	2.0
6.0	3.46	2.75	6.0	5.0
6.8	3.93	2.95	5.0	5.0
8.2	4.73	3.33		
Depth to moho			26.0	20.0

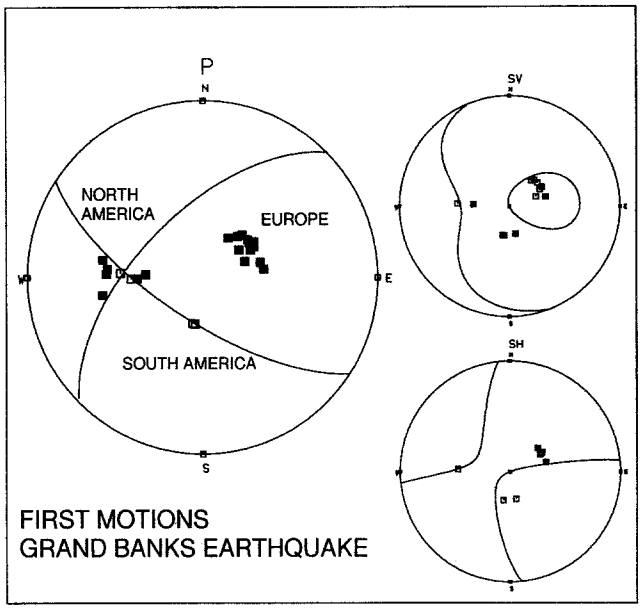

Figure 3. Focal mechanism (lower-hemisphere projection) derived from first-motion data (*P, SH,* and *SV*). Positive first motions (compressional *P, SV* toward the station, and *SH* clockwise with respect to station) are shown by filled symbols; negative first motions are indicated by open symbols. First motions at individual stations are summarized in Table 3. Note that the preferred solution is slightly different from the first-motion mechanism.

Europe. The two South American stations (LPB, SUC) are dilatational. The southwest-striking plane is constrained by the North American data. The other plane is constrained by both the North and South American data. If any of the apparently dilatational records are actually compressional, a wider range of solutions is possible, although the main features do not significantly change. Instrument polarities were marked on all the dilatational records (AAM, CHI, LPB, SUC) by the original station operators, and that of a CHI record from 1925 was consistent with polarities inferred from the mechanism of the 1925 Charlevoix, Quebec, earthquake (Bent, 1992). Therefore, they are assumed, although not proven, to be correct. The subsequent modeling efforts did not suggest that any of the assumed polarities were incorrect.

It should also be noted that the landslide mechanism of Hasegawa and Kanamori (1987) (as well as the double-couple solutions they rejected) misfits the *P*-wave first motions at AAM and CHI. However, they used only the data from AAM and probably assumed the instrument polarity was incorrect.

Both *SV* and *SH* nodal planes run through central North America. The European stations have consistent *SV* motions but are mixed with respect to *SH,* suggesting that an *SH* node passes through Europe, although the *SH* nodal plane for the best solution runs through southern rather than central Europe. The South American stations appear to be consistent with each other. If the polarities at RDJ are assumed on the basis of the *P* waves at LPB and SUC, then the *S* waves at RDJ are also consistent with these stations.

Body-Wave Forward Modeling

A wide variety of focal mechanisms were tested with emphasis on solutions in the range (within 30° of each faulting parameter) of the solution discussed above and the solutions rejected by Hasegawa and Kanamori (1987). One of the criticisms of the Hasegawa and Kanamori (1987) paper was that they tested only very specific focal mechanisms, and if they had altered some of the parameters by a few degrees perhaps an acceptable solution would have been found. Single-force sources were also tested with emphasis on solutions similar to the preferred mechanism of Hasegawa and Kanamori (1987). The best-fitting focal mechanism (strike 122° ± 5°, dip 74° ± 5°, rake 140° ± 5°) determined by forward modeling of the body waves is similar to the first-motion solution but required some modifications—4° in dip and 8° in rake. This solution represents the best overall fit to the waveforms although there are individual records that may be fit somewhat better by a different mechanism. The forward modeling solution is shown in Figure 4, but it should be noted that the synthetic seismograms contain additional subevents discussed in the "preferred solution" section of the text. A comparison of the above double-couple source and a landslide source is shown for selected stations in Figure 5.

The poorest fits tend to be at near nodal stations and can generally be improved by a modification to the mechanism within the stated uncertainties, but usually at the expense of the fit at another station. For example, the fit of the *SH* waves at UCC and KEW can be improved with a shallower dip, but at the expense of the *SH* fits at UPP and COP. The *SV* wave at UPP would be better with a higher strike-slip component, but the same solution would worsen the fit at EBR. Also, the worst-fitting stations usually have neighboring slightly less nodal stations with reasonably good fits. While the *SV* fit at UPP is less than spectacular, at nearby COP the *SV* model fits the data quite well. Similarly, the *SH* waves at GRA, POT, and HLG fit well, although there are some problems at UCC and KEW, as previously noted. It should be emphasized that the stations discussed above are all located in Europe and cover a fairly small geographic region. The modeling solution provides the best-fitting double-couple mechanism for the complete data set, but as is usually the case, there are trade-offs involved in the fit to individual records (*i.e.,* a perfect fit at one station may be sacrificed to obtain an acceptable fit at both it and an additional station). Uncertainties in the instrument responses may also contribute to data misfits, although no stations showed obvious problems with the period or damping. Magnification errors are more difficult to detect unless they are in error by more than a factor of 2, but again there were no obvious problems.

The hypocentral depth is 20 ± 2 km, placing the source well within the basement rock and near the base of the crust. Most records can be fit only by depths within this range, although a few can be fit by anything in the 15- to 25-km range. No acceptable fits were found for very shallow (<15 km) or very deep (>25 km) depths. Dewey and Gordon (1984) had obtained a depth of 19 km but with a very large uncertainty (± 17 km).

CMT Inversion

A CMT inversion of the long-period body waves (Fig. 6, Table 2) resulted in a solution that appeared very different from that obtained by forward modeling. One plane of the best-fitting double-couple solution (strike 236°, dip 41°) was oriented similarly to the southwest-striking plane (strike 225°, dip 52°, rake 20°) of the forward modeling solution but the slip angle (124°) suggested predominantly thrust rather than strike-slip motion (Fig. 7).

A number of problems, mostly related to timing uncertainties, arose during the CMT inversion. While these probably would not have occurred with modern digital data, they are likely to recur with any type of inversion of older analog data and thus merit some discussion. First, despite the fact that clock corrections were available for most of the stations, a number of records had obvious timing errors. At these stations, the data were shifted by determining the best fit to as many of the most prominent phases as possible using the expected travel times based on the assumed hypocenter of the event. Emphasis was placed on phases such as *P* and *S* for which the theoretical travel times are the most accurate. In many cases, it appeared that only the sign of the clock correction was in error (or the station used a different sign

convention); at others the source of the error was less apparent. While making these time shifts (often on the order of 10's of seconds) improved the stability and fit of the solution, the shifted records could conceivably still contain timing errors of up to several seconds. A number of additional stations appeared to have timing problems but the shift was less obvious, either because the data quality was poor, the phase was emergent, or several phases had similar amplitudes and arrival times and the correct phase could not be reliably identified. These records were excluded from further iterations. It should be emphasized that the data were time shifted only when the shift was large and obvious. Records that misfit the theoretical travel times by only a few seconds were not adjusted because it was not clear that the misfit was due to a clock error. Small timing uncertainties could be attributed to any one or more of a number of factors, including uncertainties in the epicenter, differences between the theoretical and true velocity structures, a near-nodal and/or difficult to pick arrival, or uncertainties in the station location. Despite the improved timing, the centroid location tended to drift, with the amount of movement dependent on which subset of the data set was used, suggesting that timing errors remained. Since the centroid location did not significantly affect the resulting moment

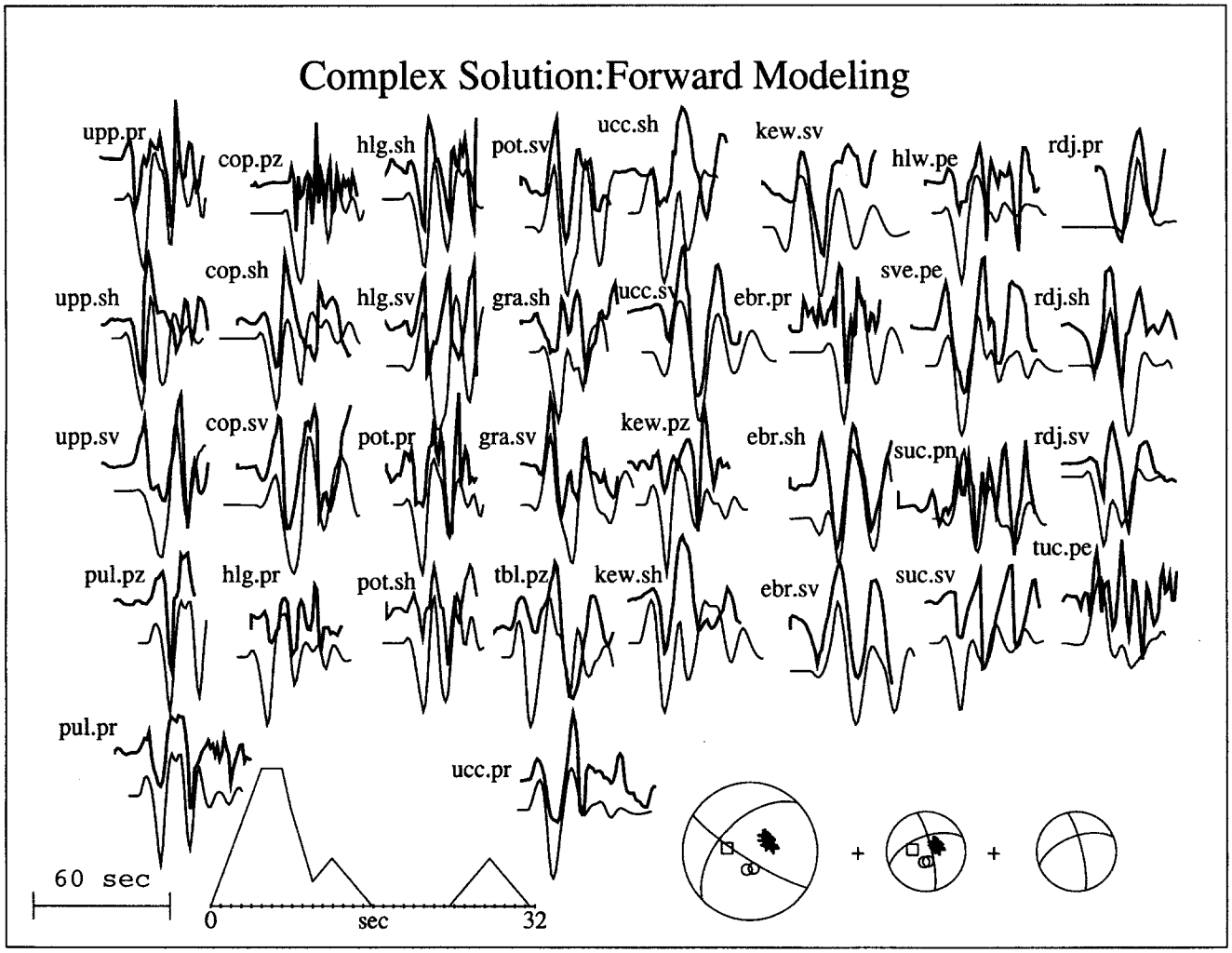

Figure 4. Body-wave data and synthetic seismograms for the preferred (complex) solution. In each pair, the observed record is the upper and darker trace. The data have not been filtered and the instrument responses have not been removed. The source time function is shown at the lower left (note that it is not plotted on the same time scale as the seismograms). The focal mechanisms of the subevents are shown at the lower right with their areas proportional to their relative moments. The square shows the location of TUC, the circles represent the South American stations (RDJ, SUC), and the plus signs indicate the European stations and HLW. All records are plotted at the same maximum amplitude, but M_W for this model at each station shown here is listed in Table 3. The traces are shown in roughly azimuthal order (clockwise from north) from top to bottom and left to right.

tensor elements, the location was fixed at the assumed epicenter listed in Table 2.

When only the best stations were used, the depth tended to stay near 20 km. When a larger data set was used, the depth tended to drift to as much as 50 km, but this result appears to be an effect of timing errors in the data. The depth had very little effect on the moment tensor elements. In any case, it does not appear that this was a very shallow event, and the depth was fixed at 20 km for the final inversion.

The best overall fits occurred for a source duration of 15 to 20 sec, although acceptable solutions could be found for a wider range of values. As for depth and centroid location, the duration had a stronger effect on the quality of the solution than on the source mechanism itself. The best solution had a corresponding M_W of 7.1. Depending on which stations were used and which parameters were fixed, M_W ranged from 6.9 to 7.2.

Five records (HLW-EW, KEW-EW, RDJ-EW, TUC-EW, and UPP-NS) provided consistent and well-fitting solutions, regardless of which (if any) of the source parameters were fixed, and whether other stations were included in the inversion. As mentioned above, the inclusion of additional stations did not significantly affect the resulting mechanism, but had a more noticeable effect on the quality of the solution and the centroid location (if not fixed). Using the solution obtained from the most reliable records, reasonable to very good fits were obtained for several additional stations, which are included in Figure 6.

Surface Waves

The short-period (20 to 40 sec) surface waves were ambiguous at best. A completely satisfactory solution was not found using the surface waves alone, and instead the Love to Rayleigh amplitude ratios were compared to those ratios expected from the mechanisms obtained by other methods (Fig. 8). Of the three models tested (forward modeling solution, CMT solution, and landslide), the solution obtained from forward modeling provided the best fit, but only mar-

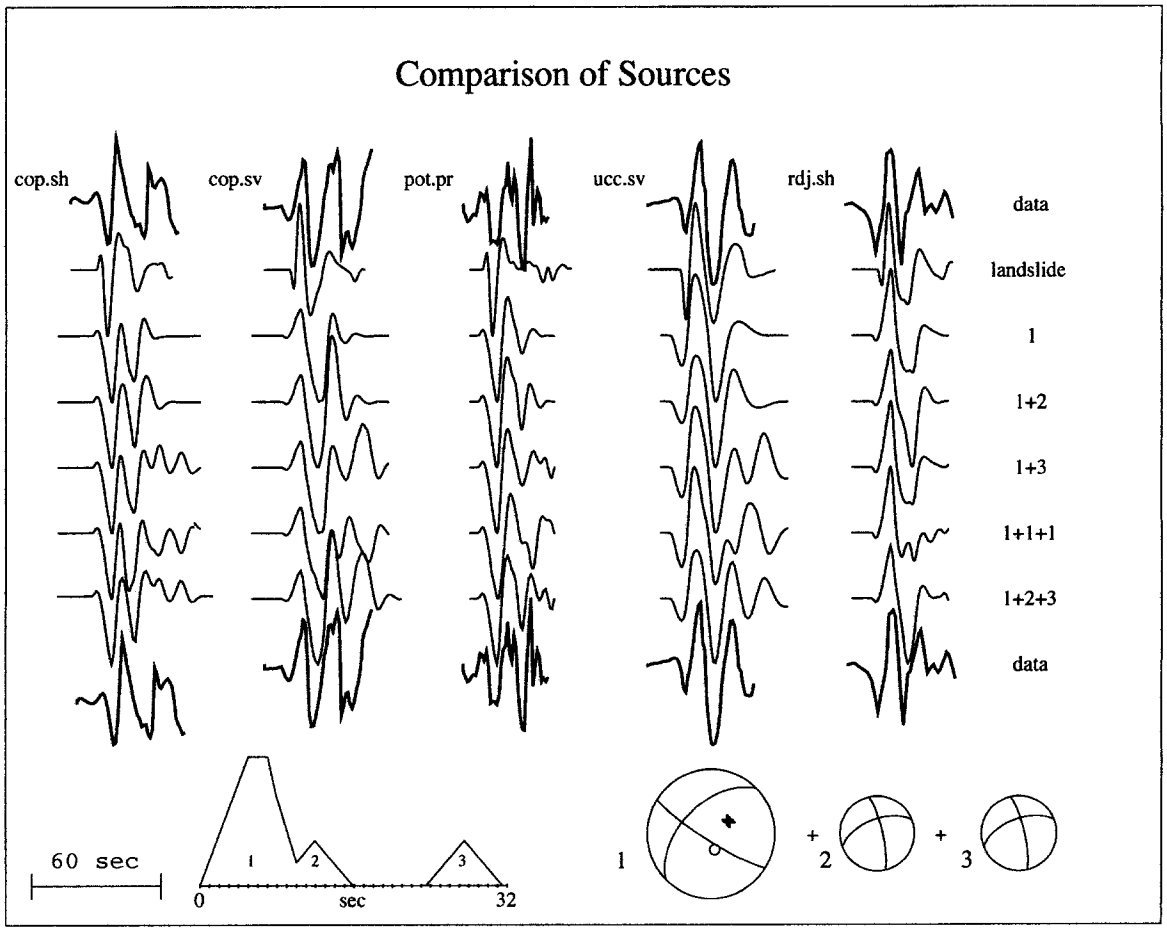

Figure 5. A comparison of simple and complex sources for selected stations and phases. The numbers on the right-hand side indicate which subevents (shown at the bottom) were included in the synthetic seismograms. For the solution 1 + 1 + 1, the time function is that shown in the lower left corner, but all three subevents have mechanism "1." The landslide mechanism is that of Hasegawa and Kanamori (1987). On the plot of focal mechanism 1, RDJ is indicated by a circle, and the European stations are shown as plus signs.

ginally so, and it misfit several stations. Hasegawa and Kanamori (1987) used the surface-wave ratios at UCC and KEW to argue for a landslide solution, and although the landslide predicts that the Love wave is the larger of the two, it underestimates the ratio (Fig. 8). Interestingly enough, all three models predict nearly the same ratio at these two stations, so they cannot be used to distinguish between source types. If a subset of the data is used, one could probably argue for any of these three models, but when the entire data set is included, the results are unclear. Figure 8 shows the ratios for a period of 40 sec, but similar ambiguities exist at 20 and 30 sec, and even if only records from stations with high magnifications in the 20 to 40-sec period range are used, one model is not significantly better than the others.

Preferred Solution

While the mechanisms obtained by forward modeling and from the CMT inversion appear very different, their resulting synthetic seismograms are remarkably similar. In many cases the waveforms are identical, and in others they are similar but out of phase with respect to each other. The S to P ratios at most stations are also very similar. Because of uncertainties in the absolute timing at most stations, the phase shift cannot be used to select one model over the other. Kikuchi and Kanamori (1991) have discussed a method for dealing with the trade-offs between timing and focal mechanism when two mechanisms are similar in waveform but phase shifted. However, they analyzed modern data where the absolute timing was presumably well constrained and the

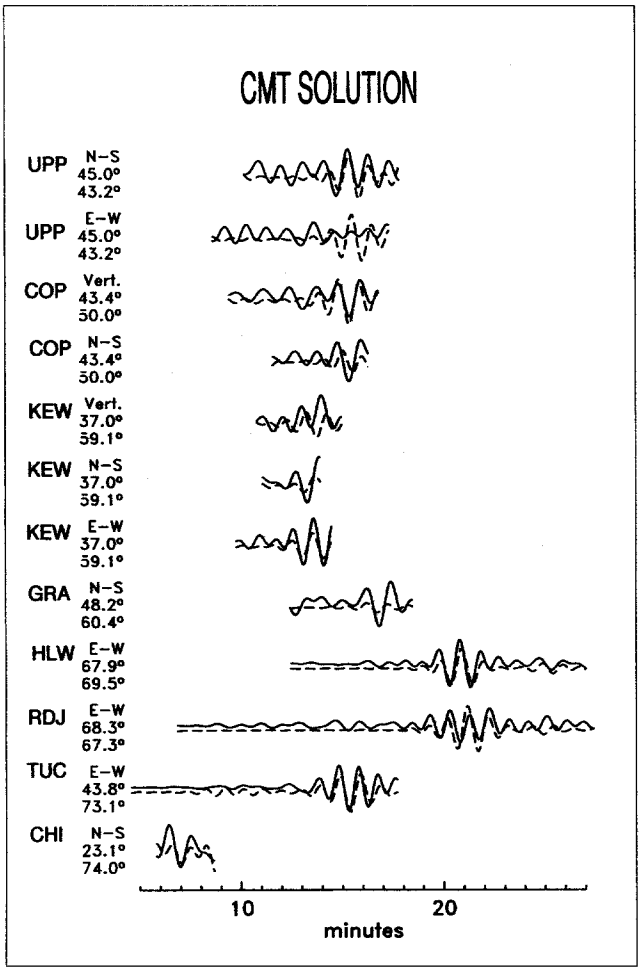

Figure 6. Data (solid lines) and synthetic seismograms calculated from the CMT inversion (dashed lines). Both the data and synthetics have been low-pass filtered with a 32-sec corner frequency. Time is measured relative to the earthquake origin time. For each station and component, the data and synthetics are plotted at the correct relative amplitude.

Table 2
Summary of Source Parameters*

Origin time	2032 18 Nov 1929 (DG)†
Epicenter	44.69° N 56.00° W (DG)†
M_S	7.2 ± 0.3
m_B	7.1 ± 0.2
M_W (CMT)	7.1 ± 0.1
M_0 (CMT)	7.3 ± 3 × 10^{19} N-m (10^{26} dyne-cm)
	First Subevent
Strike	122° ± 5°
Dip	74° ± 5°
Slip angle	140° ± 5°
Depth	20 ± 2 km
Moment	5.5 ± 3 × 10^{19} N-m
Duration	11 ± 1 sec
	Second Subevent
Strike	249° ± 10°
Dip	59° ± 10°
Slip angle	166° ± 10°
Depth	20 ± 5 km
Moment	1.9 ± 1 × 10^{19} N-m
Duration	8 ± 2 sec
Delay	7.9 ± 0.9 sec
Offset	28 ± 24 km
Azimuthal offset	≈305° (see text)
	Third Subevent
Strike	249° ± 15°
Dip	59° ± 10°
Slip angle	166° ± 15°
Depth	20 ± 5 km
Moment	1.9 ± 1 × 10^{19} N-m
Duration	8 ± 2 sec
Delay	23.5 ± 0.8 sec
Offset	100 ± 26 km
Azimuthal offset	320° ± 10°
	CMT Solution
	× 10^{19} N-m
M_{rr}	5.3 ± 1.1
M_{ff}	−0.51 ± 0.5
M_{tt}	−4.7 ± 0.5
M_{rt}	0.04 ± 0.4
M_{rf}	2.3 ± 0.5
M_{tf}	−5.2 ± 1.0
Principal axes	value × 10^{19} N-m, plunge, azimuth
T	6.1, 66.77, 232.27
N	2.4, 21.63, 29.67
P	−8.6, 8.07, 122.98

*Source parameters obtained in this study unless stated otherwise.
†DG = Dewey and Gordon (1984).

effects of timing would have a predictable effect at every station. In the case of the 1929 earthquake, the timing uncertainties require each station to be treated individually, and thus it is less apparent how to distinguish between the two mechanisms.

A closer look at the CMT results, however, indicates that the apparent discrepancy between the solutions obtained by the two methods may not be as great a problem as it first appears. While the complete CMT solution produces synthetic seismograms with a reasonable fit to the data, the best-fitting double couple obtained by this method does not. For example, the thrust mechanism is inconsistent with all of the dilatational first motions. An examination of the eigenvalues (Table 2) shows that the solution has a very high CLVD component ($\varepsilon = -0.29$) so it is not necessarily surprising that the best-fitting double couple does not fit the data as well as the complete moment tensor solution. While a high CLVD component may indicate that the source has a large non-double-couple component, it can also be an indication of source complexity (for example, see Kawakatsu, 1991). In an attempt to distinguish between the two, the solution obtained by forward modeling was converted to an equivalent moment tensor and subtracted from the CMT solution (Fig. 7). The residual moment tensor represented a nearly pure double-couple source with a strike-slip mechanism (strike 249°, dip 59°, rake 166°) different from that obtained by forward modeling and with a smaller seismic moment. The exact solution is somewhat dependent on what percentage of the total seismic moment is attributed to the first subevent. However, a change in the moment of the first subevent by a factor of 3 in either direction results in differences of less than 10° in any of the faulting parameters, although the effect on the relative moments of the subevents is more pronounced.

To ascertain whether the complex source was compatible with the waveforms, the forward modeling program was rerun. At some stations the fit of the synthetic seismograms to the data (particularly the later parts of the record) was improved, and at others the effects of the source complexity were negligible. In no instance was the complex solution worse than the simple solution.

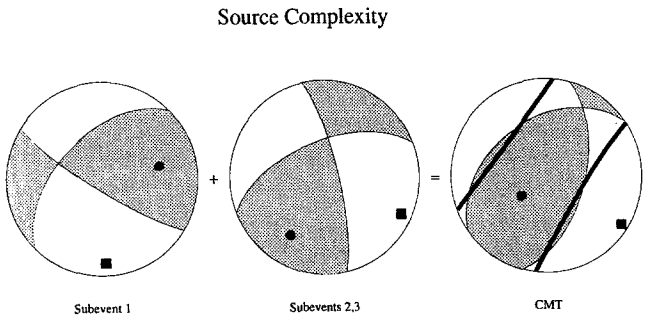

Figure 7. Fault-plane solutions of individual subevents and full CMT solution (heavy solid lines; the shaded region shows the best-fitting double-couple solution). The *P* and *T* axes are shown as squares and circles, respectively. The uncertainties associated with each of these mechanisms are indicated in Table 2.

If the nondouble couple component of the CMT solution is taken at face value, it is not indicative of a landslide source. For a near-horizontal single force, the *P*- and *S*-wave radiation patterns resemble those from a vertical (or horizontal) dip-slip double-couple source. The Love-wave radiation patterns would be significantly different, but they were not used in the CMT inversion and as discussed above, the surface waves did not strongly favor one solution over another.

To determine the time delay between the subevents, delays of 0 to 40 sec were tested using increments of 2 sec. In interval ranges where the waveform fit was improved, the increment size was decreased to obtain a more precise delay value. The most improved fits occurred for delays of 8 and 24 sec, suggesting that there were two additional subevents. A three-subevent solution provided a better or equivalent fit to a two-subevent solution at all stations modeled. The third subevent appears to have the same mechanism as the second, but because it is small and late, it is more difficult to place tight constraints on its faulting parameters. The second and third subevents are the same size, each with a moment of about one third that of the first subevent.

Figure 5 illustrates the differences between a simple double-couple solution, a landslide source, and several complex sources containing two or three subevents. Only selected stations are shown, but similar differences occur at nearby stations with instruments of comparable periods. The landslide mechanism is that of Hasegawa and Kanamori (1987) but the time function was altered to provide the best fit to the data. The first motions fit the data for all solutions shown, and with a few exceptions, the dominant frequencies of the waveforms are correctly reproduced. The principal differences between the solutions lie in their ability to fit the relative amplitudes of the waveforms and, to a lesser extent, the timing of some of later arrivals.

While in some cases, such as RDJ-*SH*, a landslide and a simple double couple produce similar synthetic seismograms, in general a double couple provides a better fit to the data. The double-couple solution can be improved by adding one or more additional subevents. For UCC-*SV*, the second subevent noticeably improves the fit of the relative amplitudes, while the third subevent has only a negligible effect. For COP-*SH*, it is the third subevent that has a more significant effect. At RDJ-*SH*, the three-subevent solution is preferable to either of the two-subevent solutions. A comparison of the two three-subevent solutions shown reveals that the fit is better when the subevents do not have the same focal mechanisms. For POT-*P*, the main difference is in the timing of the third peak. At the other stations, the relative amplitudes are more important (particularly noticeable on the UCC-*SV* and RDJ-*SH* records).

The solutions for the second and third subevents are not necessarily unique. The residual CMT solution can also be produced by adding together two or more subevents with

nonidentical focal mechanisms, and the possible combinations are essentially infinite. Most would not fit the unfiltered (intermediate-period) waveforms, but conceivably there are other combinations that would provide an adequate fit to the data. Obviously it is impractical to test every possible combination. The above solution is preferred because it is the simplest of the possible combinations, it fits both the long- and intermediate-period data, and (as discussed later) it is not unreasonable in light of what is known about the regional seismicity and tectonics. Additionally, the non-double-couple component of the residual solution is small (although somewhat dependent on the relative moment of the first subevent), which should preclude radically different mechanisms for the second and third subevents.

The surface-wave inversion assumes a simple point-source double-couple mechanism, and thus the source complexity may have contributed to the problems with the inversion. For source delays much shorter than the periods modeled, the waveforms should be dominated by the largest subevent. With delays on the order of the periods modeled, all periods would not have been affected equally, and the inversion code may have become "confused." For example, a solution that fit the 20-sec data might not have fit the 40-sec data and would not have been considered a good solution. And, as for the CMT inversion, absolute timing is important and the uncertainties in the clock errors may have also caused problems. Although the landslide appears to have been triggered by the earthquake, it may have made some contribution to the recorded waveforms. If the landslide had a slow onset relative to the earthquake, it would have had a larger effect on the long-period waves used in the surface-wave and CMT inversions than on the relatively short periods studied in the forward modeling. The fall-off of the instrument magnifications at long periods should not have been a factor because the instrument responses are removed during the inversion, and would not have been a factor in the ratio comparisons because both components would have been equally affected.

The depth of the first subevent is constrained to within 2 km by the forward modeling. The depths of the later subevents were less well constrained due to trade-offs between depth and timing, but there was no obvious change in depth between subevents (differences of more than 5 km would have been noticed). All three occurred at depths of 20 km. Since the source mechanism is predominantly strike-slip, it is not unreasonable to have a constant depth.

The first subevent had a duration of 10 to 12 sec with a 5-sec rise time. The durations of the second and third subevents are both 8 ± 2 sec, but the shapes of the source time functions are not well resolved.

To determine the spatial and temporal separation of the subevents, the apparent time delays from each station were

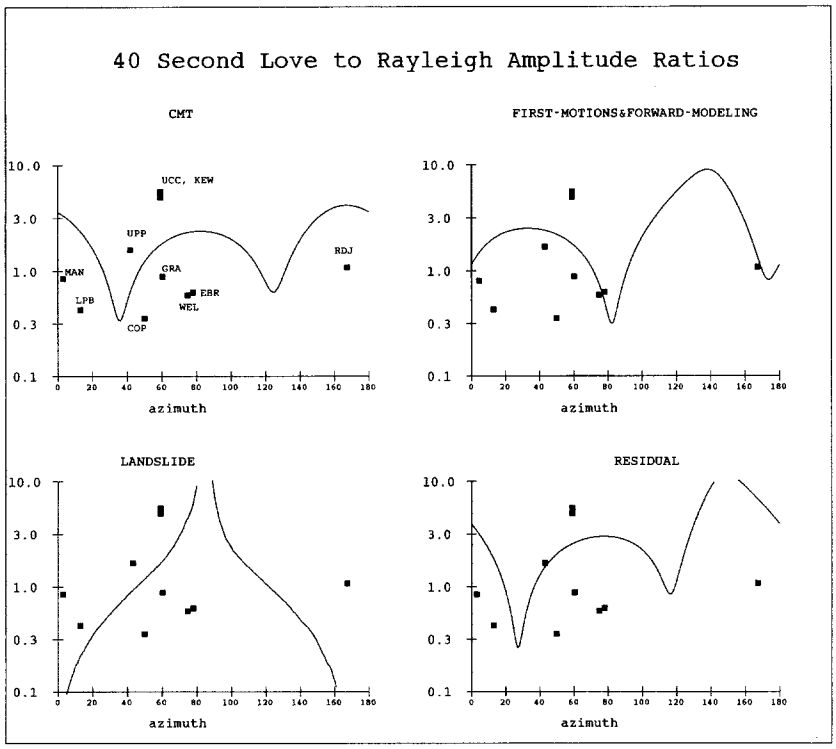

Figure 8. Love to Rayleigh amplitude ratios as a function of azimuth for 40-sec surface waves. The CMT and forward modeling solutions are those discussed in the text. The residual solution is the difference between the CMT and forward modeling solutions. The landslide mechanism is that of Hasegawa and Kanamori (1987). Note that the *y* axis is plotted on a logarithmic scale.

inverted using the least-squares method of Schwartz and Ruff (1985). Both later subevents were measured with respect to the onset time of the first subevent to avoid accumulating any uncertainties. The source separation for the third subevent is well constrained (correlation coefficient 0.67 to 0.74) and essentially independent of which portion of the data set is inverted. Using the complete data set (Fig. 9b), the offset with respect to the first subevent is 100 ± 26 km along an azimuth of 320°, with a delay of 23.5 ± 0.8 sec.

The data for the second subevent show a considerable amount of scatter and do not produce a well-constrained solution. Because the correlation coefficient was only 0.27, the inversion was rerun using only those stations where Δt was tightly constrained, but the improvement was only marginal (correlation coefficient 0.35). The calculated separation is dependent on the choice of stations. For the complete data set, the separation is 7.4 ± 6.0 km along an azimuth of 35°, whereas the reduced data set (Fig. 9a) suggests a separation of 28 ± 24 km at an azimuth of 305°. The two solutions are in better agreement with respect to the time delay—9.4 ± 0.5 sec for the complete data set and 7.9 ± 0.9 sec for the partial data set. The azimuthal separation and apparent rupture velocity of the second subevent determined from only the best-fitting stations are consistent with those determined for the third subevent, and therefore this solution is preferred, although the others cannot be completely ruled out.

Magnitude and Moment

M_S was calculated to be 7.2 ± 0.3 from measurements at 23 stations, and m_B to be 7.1 ± 0.2 from measurements at 24 stations. The magnitudes at each station are shown in Table 3. Both values are consistent with previous magnitude estimates for this earthquake. Hasegawa and Kanamori (1987), Abe (1981), and Gutenberg and Richter (1956) obtained values of 7.2 for both magnitudes. Street and Turcotte (1977) calculated M_S as 7.1. Pacheco and Sykes (1992), using an adjustment method based primarily on global seismicity rates, had listed M_S as 7.0. Within their respective uncertainties, all magnitude estimates are in agreement with each other.

Using the CMT method, a moment of 7.3 × 10^{19} N-m (or 10^{26} dyne-cm) was determined which corresponds to an M_W of 7.1 (±0.1). The sum of the subevent moments is slightly higher (5.5 × 10^{19} + 1.9 × 10^{19} + 1.9 × 10^{19}) and corresponds to an M_W of 7.2 (±0.3; Table 3). The CMT moment magnitude is preferred because it is more tightly constrained, but the difference between the values obtained by the two methods is not significant. The short-period (20 to 40 sec) surface waves are also consistent with a moment in the 6 to 8 × 10^{19} N-m range.

Discussion

The directivity analysis, which indicated that the two later subevents occurred to the northwest of the first sub-

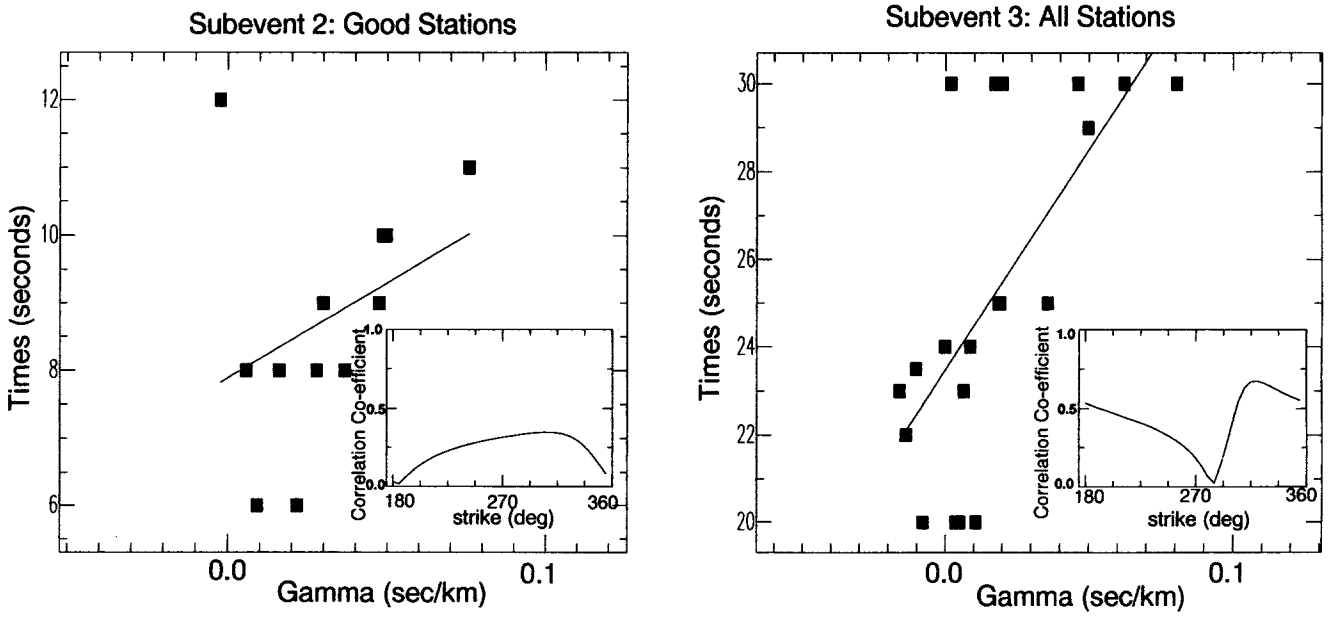

Figure 9. Determination of the separation between subevents for the second subevent (left) using only data from the best-fitting stations, and the third subevent (right) using all available data. Both are measured relative to the first subevent. The term Γ is the directivity parameter as described by Schwartz and Ruff (1985), and is related to the phase velocity and station azimuth. The observations are shown as squares and the line shows the best least-squares fit to the data. In the insets, the correlation coefficients are shown as a function of azimuthal separation.

event, suggests that the first subevent ruptured along the northwest–southeast-striking nodal plane and therefore the fault slipped in a right-lateral sense. The rupture was predominantly unilateral although the data do not preclude some additional rupture toward the southeast. Because the northwest-striking nodal planes of the second and third subevents indicate left-lateral rupture (*i.e.*, opposite sense of first subevent), they are probably not the fault planes, and these subevents most likely ruptured along the northeast–southwest-striking planes oblique to the first subevent. Backslip along the initial fault plane cannot be completely ruled out, however, because the data are insufficient to determine the rupture directions of the later subevents.

The 1929 earthquake cannot be associated with a particular fault or structure with any certainty, but there are a number of correlations that can be made between the source parameters and the regional tectonics and seismicity. The strike of the presumed fault plane of the first and largest subevent is consistent with a landward extension of the Newfoundland Fracture Zone, and also with the trend of the Laurentian Channel. The presumed rupture planes of the later subevents are roughly parallel to the continental margin.

The seismicity in the Laurentian Channel region (Fig. 1) consists of two or three clusters of earthquakes each trending roughly northwest–southeast and separated from each other also in a northwest–southeast direction. This trend cor-

Table 3
Summary of Magnitudes and First Motions

STN	M_s	M_w*	m_B (*PZ*)	m_B (*PR*)	m_B (*SH*)	First Motion† (*P*)	(*SV*)	(*SH*)
AAM						−	−	−
BFF				7.3		+		
BOH	6.7			7.1	6.9			
BOM	7.2			7.3	7.2			
CHI				7.1	7.5	−		
COP	7.1	7.4	7.3	6.9	7.2	+	−	+
CRT	7.2			7.3	7.3	+		
EBR	7.2	7.4		7.1	6.9	+	−	+
FBR	6.8			6.9	7.3			
FOR						+		
GRA	7.6	7.3		7.3	7.0		−	−
HLG	7.2	7.5		6.8	7.0			
HLW	7.1			7.4	7.4	+	+	
KEW		7.2	7.3	7.4	7.0	+	−	−
LPB	7.1			7.5	7.0	−	+	−
LUN	7.6							
MAN	7.0							
MEL	7.2							
OTT			7.0			+		
PER	7.4							
POT	6.9	7.3		7.5	7.2	+		
PUL		6.9	6.9			+	−	
RDJ	7.2	6.9		7.2	7.3	−	+	−
SIT	7.6							
SLM						+		
STO	7.1			7.0	7.0	+		
SUC	6.6					−	+	
SVE				6.8	6.5	+		
TBL		6.6	6.7	6.8		+		
TNT				6.7		+		
TOK	7.1							
TUC	7.3			6.9	7.0	+	+	
UCC	7.6	7.1	7.0		7.1	+	−	−
UPP	6.8	7.2		7.1		+	−	
Mean	7.16 ±0.28	7.16 ±0.27	7.03 ±0.23	7.11 ±0.25	7.09 ±0.22			
Mean (all m_B)		7.10 ±0.23						

*Based on forward modeling; M_W from CMT inversion is 7.1 ± 0.1.

†Sign convention: + indicates compression for *P* waves, motion toward the station for *SV*, and motion clockwise with respect to the station for *SH*.

responds to the fault strike and rupture direction for the first and largest subevent. The length of the southernmost cluster (where the 1929 event occurred) is about the same length as the 1929 rupture calculated from the subevent separation. The spatial correlation of recent seismic activity to the presumed fault planes of the 1929 event suggests that the interpretation of Adams *et al.* (1984) that the recent events are aftershocks of the 1929 earthquake may be correct. It is not clear, however, whether the 1975 earthquake, which lies in a different cluster of events and has a subcrustal origin, is directly related to the 1929 earthquake.

Based on the best-available velocity model for the Laurentian Channel region, the hypocenter of the 1929 earthquake lies near the base of the crust. While a shallow crustal source can be ruled out, the combined uncertainties in the focal depth, velocity structure, and epicenter may allow an uppermost mantle source.

The strike-slip nature of the 1929 earthquake suggests that the associated tsunami was likely caused, or at the minimum, exacerbated by the submarine slump. Since the return period for a tectonic earthquake along the Atlantic margin of eastern Canada is assumed to be about an order of magnitude less than the time required for sufficient sediment to accumulate to cause a similar-sized landslide (Hasegawa and Kanamori, 1987), it is important to understand the tsunami potential from tectonic earthquakes alone. Using the preferred 1929 mechanism, the vertical seafloor displacement was modeled (after Mansinha and Smylie, 1971). There are some uncertainties in the actual fault dimensions and offsets, particularly for the later subevents. A minimum fault length for the first subevent can be assumed based on the separation of the later subevents. The fault lengths are unknown for the two smaller subevents. The seismic moment is well determined for all the subevents, but in all cases there are tradeoffs between fault width and displacement. Therefore, models were tested for several combinations of fault size (length and width), vertical extent, and displacement. The displacement pattern was not significantly different for any of the models tested, and in all cases, the maximum seafloor displacement was less than 20 cm. The seafloor displacement for a fault extending from the surface to 20 km is shown in Figure 10. Note that there is no evidence that the fault actually ruptured the surface, but this model is shown because it represents the "worst case" scenario.

From the seafloor displacement, the volume of water displaced by the earthquake can also be calculated. For the model shown in Figure 10, the volume is roughly 7×10^8 m^3, which is one to two orders of magnitude less than than the volume of water displaced by other tsunamigenic earthquakes summarized by Abe (1979) and Kanamori (1972). The volume of sediment (and therefore water) displaced by the slump is in the range of water displacement for the tsunamigenic earthquakes, indicating that almost all of the displaced water (and therefore the tsunami) was related to the slump and not the earthquake. These comparisons combined with the fact that the effects of the 1929 tsunami were exacerbated by its coincidence with high tide in Newfoundland (Doxsee, 1948), suggest that until the sediment supply is replenished, the tsunami hazard in this region from a repeat of the 1929 earthquake is very small. Although it might have a measurable effect, it would be unlikely to be destructive. Elsewhere along the eastern seaboard, an earthquake with a similar mechanism would probably be tsunamigenic only in regions of large sediment accumulation.

Because the 1975 Laurentian Channel earthquake had primarily a thrust mechanism, the possibility of a large thrust earthquake in this region cannot be completely ruled out. The seafloor displacement was also calculated for an earthquake with a mechanism similar to that of the 1975 earthquake, but with a seismic moment and depth comparable to the 1929 earthquake. In this case, the maximum seafloor displacement was increased by almost a factor of 2 to 35 cm, with the maximum displacement occurring over a wider area, and the displaced water volume is on the order of 10^9 m^3, again relatively small compared to other tsunamigenic earthquakes. Thus, it appears that a tsunami from a future local earthquake in the 1929 epicentral region is unlikely unless the magnitude of the earthquake is much greater than previous earthquakes, the focal mechanism is very different (pure dip-slip motion on a near-vertical fault) from both the 1929 and 1975 earthquakes, or the sediment has had time to reaccumulate to pre-1929 levels.

Conclusions

A double-couple solution consistent with the observed waveforms and first motions has been found for the 1929 Grand Banks earthquake, confirming that the triggering mechanism was an earthquake and not a landslide. A focal depth of 20 km also precludes a landslide source mechanism. Results of a detailed waveform modeling study have shown that the earthquake had a complex source, with the best solution consisting of three subevents. The first and largest subevent had a strike-slip double-couple mechanism (strike 122°, dip 74°, rake 140°). The simplest solution consistent with the data suggests that the later subevents were also strike-slip double couples but with different mechanisms (both strike 249°, dip 59°, rake 166°) from the first subevent. The solutions for the second and third subevents are not necessarily unique, and it is possible that other combinations of mechanisms (double couple and/or single force) would satisfy the waveform data.

A directivity analysis suggested that the first subevent ruptured right laterally along a fault trending more or less parallel to the Newfoundland Fracture Zone and Laurentian Channel. The third and probably also the second subevent were offset to the NW of the first, and probably ruptured right laterally along faults subparallel to the trend of the continental slope. The data preclude the determination of rupture direction for the later subevents. To a first approximation, both the strike orientations and subevent separations are consistent with the trend of the seismicity and known

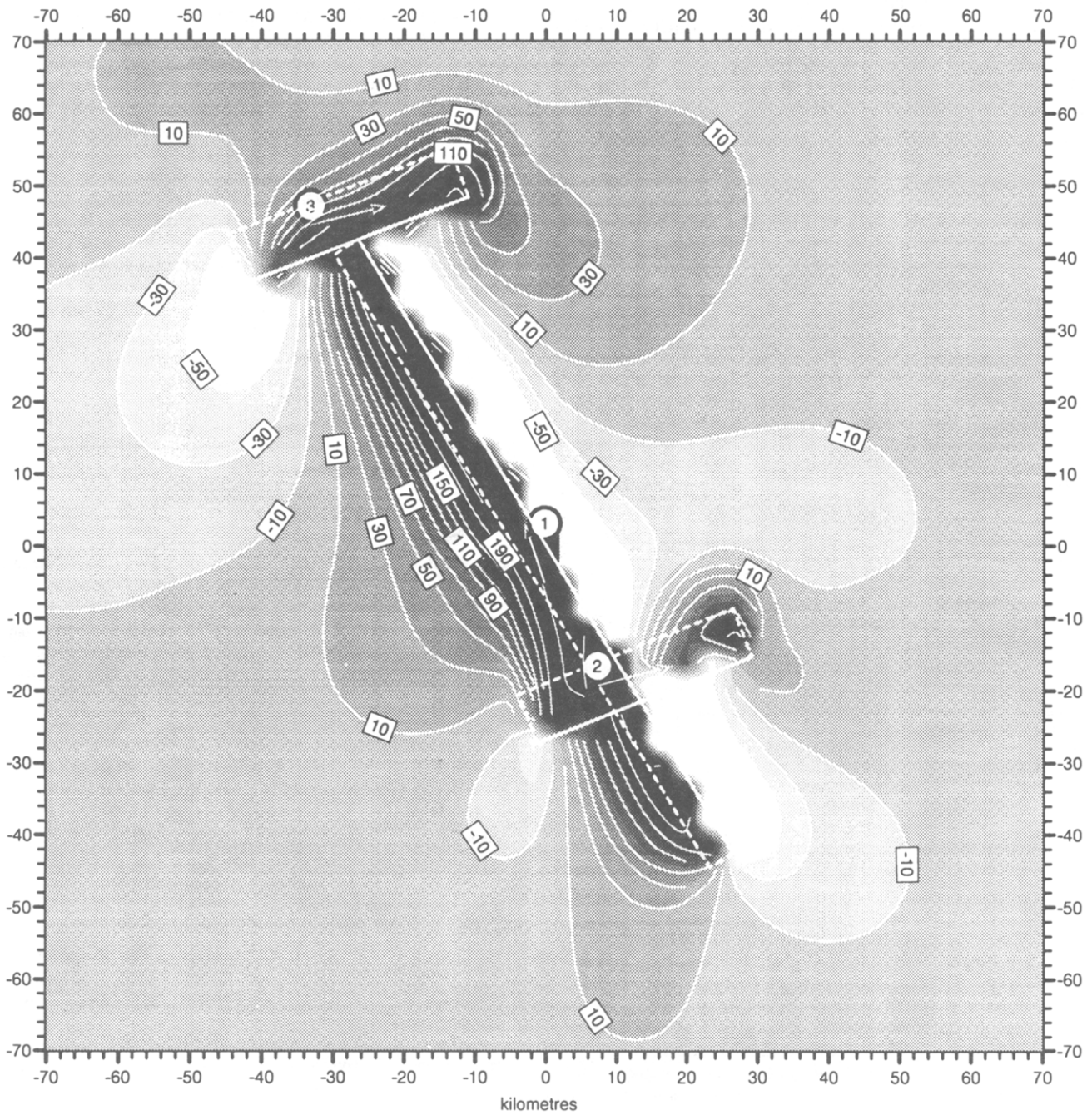

Figure 10. Seafloor displacement for the 1929 earthquake for a fault extending from the surface to 20 km (although there is no evidence that the 1929 earthquake ruptured the surface). Neither the large-scale properties of the displacement pattern nor the maximum displacement is significantly changed for other choices of fault width and depth extent. The contour labels shown in boxes give the seafloor displacement in millimeters. The numbers in circles indicate the subevent number. The boxes outlined by dashed lines show the surface projections of the faults. Horizontal distances (in kilometers) are measured relative to the center of the largest fault. The epicenter is at the southeast end of fault 1. For these calculations, bilateral rupture was assumed for the second and third subevents, but their actual rupture directions cannot be resolved.

structures in the region, although the earthquake cannot be placed on a specific fault with certainty.

The seismic moments of the second and third subevents are each one third that of the first, and the sum of the subevent moments is equivalent to an M_W of 7.2, which is in good agreement with the M_W of 7.1 obtained from the long-period data using the CMT inversion, and with the M_S of 7.2 and m_B of 7.1 obtained from direct measurements of the seismograms.

Models of the seafloor displacement expected from an earthquake with the source properties discussed above suggest that a repeat of the 1929 earthquake in the future would be unlikely to generate a destructive tsunami until the sediment supply on the continental slope has been replenished. A similar earthquake elsewhere along the eastern seaboard would probably not be tsunamigenic unless it triggered the slumping of long-accumulated sediment. Tsunamis cannot be completely ruled out for much larger earthquakes or earthquakes with focal mechanisms different from both the 1929 and 1975 earthquakes.

Acknowledgments

Seismograms not in the original collection were supplied by N. A. Sergeyeva, O. E. Starovoit, J. Taggart, and R. Wahlström. I would like to thank Göran Ekström and Misha Salganik for their help with the CMT inversion, and Stephen Halchuk for showing me how to run the seafloor displacement code. Helpful reviews were provided by John Adams, Anne Stevens, and two anonymous reviewers. Geophysics Division, Geological Survey of Canada Contribution Number 53093.

References

Abe, K. (1979). Size of great earthquakes of 1837–1974 inferred from tsunami data, *J. Geophys. Res.* **84,** 1561–1568.

Abe, K. (1981). Magnitude of large shallow earthquakes from 1904 to 1980, *Phys. Earth Planet. Interiors* **27,** 72–92.

Adams, J. (1986). Changing assessment of seismic hazard along the southeastern Canadian margin, in *Proc. of the 3rd Canadian Conference of Marine Geotechnical Engineering,* St. John's, Newfoundland, 41–53.

Adams, J. and P. Basham (1989). The seismicity and seismotectonics of Canada east of the Cordillera, *Geosci. Canada* **16,** 3–16.

Adams, J., I. Reid, and P. W. Basham (1984). Historical seismicity, 1983 OBS experiment and seismic hazard along the southeastern Canadian margin, in *18th Annual Congress Canadian Meteorological and Oceanographic Society Joint Program with Abstracts,* 67–68.

Bent, A. L. (1992). A re-examination of the 1925 Charlevoix, Québec, earthquake, *Bull. Seism. Soc. Am.* **82,** 2097–2113.

Bent, A. L. (1994). Seismograms for historic Canadian earthquakes: the 18 November 1929 Grand Banks earthquake, *Geol. Surv. Canada Open-File Rept. 2563,* 36 pp.

Charlier, C. and J. M. Van Gils (1953). *Liste de Stations Seismologigues Mondiales,* Obs. Royal de Belgique, Uccle.

Dewey, J. W. and D. W. Gordon (1984). Map showing recomputed hypocenters of earthquakes in the eastern and central United States and adjacent Canada, 1925 to 1980, Dept. of the Interior, U.S. Geological Survey, Misc. Field Studies, Map MF-1699. 39 pp.

Doxsee, W. W. (1948). The Grand Banks earthquake of November 18, 1929, *Publ. Dom. Obs.* **7,** 323–335.

Drake, C. L. and H. P. Woodward (1963). Appalachian curvature, wrench faulting and offshore structures, *New York Acad. Sci. Trans. Ser. II* **26,** 48–63.

Dziewonski, A. M. and D. L. Anderson (1981). Preliminary reference Earth model, *Phys. Earth Planet. Interiors* **25,** 297–356.

Dziewonski, A. M. and J. H. Woodhouse (1983). An experiment in systematic study of global seismicity: centroid-moment tensor solutions for 201 moderate and large earthquakes of 1981, *J. Geophys. Res.* **88,** 3247–3271.

Dziewonski, A. M. and R. L. Woodward (1992). Acoustic imaging at the planetary scale, in *Acoustical Imaging,* H. Emert and H.-P. Harjes (Editors), Vol. 19, Plenum Press. New York, 785–797.

Dziewonski, A. M., T. Chou, and J. H. Woodhouse (1981). Determination of earthquake source parameters from waveform data for studies of global and regional seismicity, *J. Geophys. Res.* **86,** 2825–2852.

Ebel, J. E., P. G. Somerville, and J. D. McIver (1986). A study of the source parameters of some large earthquakes of northeastern North America, *J. Geophys. Res.* **91,** 8231–8247.

Fletcher, J. B., M. L. Sbar, and L. R. Sykes (1978). Seismic trends and travel-time residuals in eastern North America and their tectonic implications, *Geol. Soc. Am. Bull.* **89,** 1656–1676.

Futterman, W. I. (1962). Dispersive body waves, *J. Geophys. Res.* **67,** 5279–5291.

Gussow, W. C. (1982). The Grand Banks earthquake of 1929, *Disc. Geosci. Canada* **9,** 122–123.

Gutenberg, B. and C. F. Richter (1956). Magnitude and energy of earthquakes, *Ann. Geofis.* **9,** 1–15.

Hasegawa, H. S. and H. Kanamori (1987). Source mechanism of the magnitude 7.2 Grand Banks earthquake of November 1929: double couple or submarine landslide? *Bull. Seism. Soc. Am.* **77,** 1984–2004.

Hasegawa, H. S. and R. B. Herrmann (1989). A comparison of the source mechanisms of the 1975 Laurentian Channel earthquake and the tsunamigenic 1929 Grand Banks event, in *Earthquakes at North-Atlantic Passive Margins: Neotectonics and Postglacial Rebound,* S. Gregersen and P. Basham (Editors), Kluwer Academic Publishers, Dordrecht, Netherlands, 547–562.

Herrmann, R. B. (1979). Surface wave focal mechanisms for eastern North American earthquakes with tectonic implications, *J. Geophys. Res.* **84,** 3543–3552.

Hughes Clarke, J. H. (1990). Late stage slope failure in the wake of the 1929 Grand Banks earthquake, *Geo-Marine Lett.* **10,** 69–79.

Kanamori, H. (1972). Mechanism of tsunami earthquakes, *Phys. Earth Planet. Interiors* **6,** 346–359.

Kanamori, H., J. W. Given, and T. Lay (1984). Analysis of body waves excited by the Mount St. Helen's Eruption of May 18, 1980, *J. Geophys. Res.* **89,** 1856–1866.

Kawakatsu, H. (1991). Enigma of earthquakes at ridge-transform-fault plate boundaries-distribution of non-double couple parameter of Harvard CMT solutions, *Geophys. Res. Lett.* **18,** 1103–1106.

Keen, C. E. and R. D. Hyndman (1979). Geophysical review of the continental margins of eastern and western Canada, *Can. J. Earth Sci.* **16,** 712–747.

Keen, C. E. and R. T. Haworth (1984a). North American continent ocean transects program, Transect D3, rifted continental margin off Nova Scotia: offshore Eastern Canada, *Geol. Soc. Am.,* 7 pp. and map.

Keen, C. E. and R. T. Haworth (1984b). North American continent ocean transects program, Transect D2: transform margin south of Grand Banks: offshore Eastern Canada, *Geol. Soc. Am.,* 6 pp. and map.

Kikuchi, M. and H. Kanamori (1991). Inversion of complex body waves—III, *Bull. Seism. Soc. Am.* **81,** 2335–2350.

King, L. H. and B. MacLean (1970). Origin of the outer part of the Laurentian Channel, *Can. J. Earth Sci.* **7,** 1470–1484.

Kumarepeli, P. S. (1970). Monteregian alkalic magmatism and the St. Lawrence rift system in space and time, *Can. Mineral* **10,** 421–431.

Kumarepeli, P. S. and V. A. Saull (1966). The St. Lawrence Valley system: a North American equivalent of the East African Rift Valley system, *Can. J. Earth Sci.* **3,** 639–658.

Langston, C. A. and D. V. Helmberger (1975). A procedure for modeling shallow dislocation sources, *Geophys. J. R. Astr. Soc.* **42,** 117–130.

Mansinha, L. and D. E. Smylie (1971). The displacement fields of inclined faults, *Bull. Seism. Soc. Am.* **61,** 1433–1440.

Pacheco, J. F. and L. R. Sykes (1992). Seismic moment catalog of large, shallow earthquakes, 1900–1989, *Bull. Seism. Soc. Am.* **82,** 1306–1349.

Piper, D. J. W. and A. E. Aksu (1987). The source and origin of the 1929 Grand Banks turbidity current inferred from sediment budgets, *Geo-Marine Lett.* **7,** 177–182.

Piper, D. J. W., A. N. Shor, J. A. Farre, S. O'Connell, and R. Jacobi (1985). Sediment slides and turbidity currents on the Laurentian Fan: sidescan sonar investigations near the epicenter of the 1929 Grand Banks earthquake, *Geology* **13,** 538–541.

Piper, D. J. W., A. N. Shor, and J. E. Hughes Clarke (1988). The 1929 "Grand Banks" earthquake, slump, and turbidity current, *Geol. Soc. Am. Special Paper 229,* 77–92.

Reid, I. (1987). Crustal structure of the Nova Scotian margin in the Laurentian Channel region, *Can. J. Earth Sci.* **24,** 1859–1868.

Schwartz, S. Y. and L. J. Ruff (1985). The 1968 Tokachi-Oki and the 1969 Kurile Islands earthquakes: variability in the rupture process, *J. Geophys. Res.* **90,** 8613–8626.

Street, R. and F. T. Turcotte (1977). A study of northeastern North American spectral moments, *Bull. Seism. Soc. Am.* **67,** 599–614.

Tsai, Y. B. and K. Aki (1970). Precise focal depth determination from amplitude spectra of surface waves, *J. Geophys. Res.* **75,** 5729–5743.

Williams, H., M. J. Kennedy, and E. R. W. Neale, Coordinators (1972). The Appalachian Structural Province, in *Variations in Tectonic Styles in Canada,* R. A. Price and R. J. W. Douglas (Editors), *Geol. Assoc. Can. Spec. Paper* **12,** 181–261.

Wilson, J. T. (1940). The Love waves of the south Atlantic earthquake of 28 August 1933, *Bull. Seism. Soc. Am.* **30,** 273–301.

Wood, H. O. (1921). A list of seismologic stations of the world, *Bull. Natl. Res. Council* **2,** 397–538.

Geophysics Division
Geological Survey of Canada
Ottawa, Ontario, Canada K1A 0Y3

Manuscript received 11 April 1994.

Appendix
Seismograms for 1929 Grand Banks Earthquake

Station	Δ (deg)	Az. (deg)	Instr*	Comps	τ* (sec)	ε*	V*	Source†
Abisko (ABI)	44	31	G	Z,N,E	11.9	—	1100	Wo
Alma-Ata (AAA)	83	33	N	N,E	3.0	8.8	360	S
Ann Arbor (AAM)	20	273	W	N,E				
Barcelona (FBR)	42	73	M	N	10	25	78	S,Wo
				E	10	19	65	S,Wo
Böhmen (BOH)	45	58	M	N	9.4	40	100	S
			Be	E	12	ℓ	110	S
Bombay (BOM)	101	49	MS	N	12	20	250	S
Buffalo (BFF)	16	272	W	N	3.7	5	80	S
				E	4.8	5	80	S
Chicago (CHI)	23	274	MS	N,E	12	20	150	S
Copenhagen (COP)	43	50	W	Z	5.8	4.1	160	S
			N	9.8	4.6	220	S	
				E	9.6	4.5	195	S
			WA	N	11	aper		S
			MS	E	12	20	300	S
Ebro/Tortosa (EBR)	41	75	MS	N	20	10	7	S
			M	N	14.8	2.3	194	S
				E	7.5	2	100	S
Fordham (FOR)	14	260	W	N,E			45	B
Granada/Cartuja (CRT)	40	82	Blm	Z	6			C
			Ber	N	5.4	4	760	S
				E	4		590	S
Graz (GRA)	48	60	W	N	10	4.5	164	S
				E	9.9	4.3	181	S
Helgoland (HLG)	41	53	W	N	11.6	3.9	126	S
				E	12.5	5.3	153	S
Helwan (HLW)	68	69	MS	E	12	20	250	Wi
Kew (KEW)	37	59	G	Z	12.9	—	308	S,B
				N	25.5	—	280	S,E
				E	24.7	—	280	S,E
Kobe (KOB)	100	351	W	NE	5	2.2	90	S
				NW	3	1.8	94	S
Kodaikanal (KOD)	111	50	Mi	E	16	1	10	S
La Paz (LPB)	62	193	Bi	E	12	3	300	S
				N	14	3	180	S
Lund (LUN)	44	50	W	N,E	9	3.5	190	S

Appendix—*Continued*
Seismograms for 1929 Grand Banks Earthquake

Station	Δ (deg)	Az. (deg)	Instr*	Comps	τ* (sec)	ε*	V*	Source†
Manila (MAN)	121	3	W	N	7.82	4.7	156	S
				E	7.85	5.5	155	S
Melbourne (MEL)	162	290	MS	E	12	20	250	S
Mt. Hamilton (MHC)	49	286	W	N,E			80	S,ST
Ottawa (OTT)	14	280	W	Z	6	7	160	B
			B	N	5.2	2	120	B
				E	6.9	14	120	B
Oxford (OXD)	36	59	MS	N,E	12	20	250	S
Perth (PER)	152	29	MS	N	12	20	250	S
Potsdam (POT)	45	54	W	N	9.8	4	250	S
				E	6.0	2.5	330	S
Pulkovo (PUL)	51	40	G	Z	14.0	—	1428	S
				N	14.8	—	1587	S
				E	13.9	—	1392	S
Rio de Janeiro (RDJ)	68	167	MS	N,E	12	20	250	S
Scoresby Sund (SCO)	31	22	GW	Z	10	—	600	S
				N	12.4	—	770	S
				E	11.9	—	750	S
Seven Falls (SFA)	11	288	WA	E	1	15	2500	B
			MS	E	12	20	250	B
Simferopol (SIM)	60	55	N	N	2.0	90	400	S,C
Sitka (SIT)	49	315	BO	N	17	1	10	S,ST
St. Louis (SLM)	26	269	WA	N	10.2	1	400	B
				E	9.5	1	360	B
Stonyhurst (STO)	35	55	MS	E	12	20	150	S
Sucre (SUC)	64	190	Bi	N	12	2	300	S
Sverdlovsk (SVE)	66	33	G	E	25.0	—	2048	S
Sydney (SYD)	156	289	MS	E	19			S
Tblisi/Tiflis (TBL)	69	52	G	Z	12.3	—	1156	S
				N	12.4	—	1402	S
				E	12.4	—	1511	S
Tokyo (TOK)	99	347	BO	N,E	4.5		120	S
Toronto (TNT)	17	275	MS	N,E	12.0	20	150	S
Tucson (TUC)	44	273	WA	E	10	28.7	435	S
Tyosi/Chosi (CHO)	99	346	W	N	3.7	4	76	S
				E	6.3	7	91	S
Uccle (UCC)	40	59	G	N	25	—	860	S
				E	25		820	S
			W	Z,E	4.8	2.8	150	S
Uppsala (UPP)	45	43	W	N,E	8.7	3.5	190	S
Wellington (WEL)	143	258	MS	N	10.15	25	150	S
				E	10	19	150	S

*B = Bosch, BO = Bosch–Omori, Be = Belar, Ber = Berchmans, Bi = Bifilaire, Blm = Belamino, G = Galitzin, GW = Galitzin–Wilip, M = Mainka, MS = Milne–Shaw, Mi = Milne, N = Nikiforov, W = Wiechert, WA = Wood–Anderson; τ = pendulum period, ε = damping ratio, V = static magnification for mechanical instruments and maximum magnification for electromagnetic instruments. For electromagnetic instruments, such as the Galitzin, it is assumed that the pendulum and galvanometer periods are equal and that the damping constant for each is 1.0.

†S = station (record), B = station bulletin, C = Charlier and Van Gils (1953), E = Ebel *et al.* (1986), ST = Street and Turcotte (1977), Wi = Wilson (1940), Wo = Wood (1921).